Pergamon

Int. J. Heat Mass Transfer. Vol. 40, No. 12, pp. 2901–2911, 1997

Printed in Great Britain
0017–9310/97 $17.00 + 0.00

PII: S0017–9310(96)00326–2

Effects of a geometric perturbation on buoyancy induced flow and heat transfer in a cylindrical annulus

S. V. IYER and K. VAFAI†

Department of Mechanical Engineering, The Ohio State University, Columbus, OH 43210, U.S.A.

(*Received* 25 *June* 1996 *and in final form* 10 *September* 1996)

Abstract—A numerical investigation has been carried out to study the effect of a geometric perturbation on the three-dimensional buoyancy-driven flow and heat transfer in an annular cavity with impermeable end walls. The numerical scheme used in the present study is based on a Galerkin method of finite element formulation. The nature of the three-dimensional flow-field has been analyzed in detail. The local and average Nusselt numbers were obtained for a wide range of Rayleigh numbers, and the heat transfer performance was compared with that for the closed horizontal annulus without a perturbation. The effect of variation of a number of key geometric parameters of the perturbation on the overall heat transfer behavior has been studied. Some of the key features due to the introduction of the perturbation, and qualitative and quantitative effects of the perturbation within the annulus are discussed. It is shown that the introduction of the geometric perturbation can lead to a large increase in the overall heat transfer within the annulus. © 1997 Elsevier Science Ltd.

1. INTRODUCTION

The natural convection flow and heat transfer within a cylindrical annulus has received considerable attention in recent years. This is primarily because of the numerous applications such as nuclear reactor design, cooling of electronic components, electric transmission cables, aircraft insulation, etc.

Many theoretical and experimental investigations have been carried out. In most of the earlier studies, a two-dimensional (2-D) model was used in which the annulus is assumed to be infinitely long so that convection could be assumed to be within the transverse plane only. The work by Kuehn and Goldstein [1] constitutes a classical work for these types of studies. For many practical applications where the annulus has a finite axial length, the viscous shearing effects at the end walls necessitate a full three-dimensional (3-D) analysis. In the past decade, there have been some studies which considered the 3-D fluid flow and heat transfer in concentric cylindrical annuli. However, although the 3-D free convection between concentric cylinders is well understood, a comprehensive literature survey revealed that very few geometric modifications to the horizontal concentric cylindrical annuli have been considered. This paper presents the results of an investigation concerning the buoyancy-driven flow and heat transfer in a concentric annulus with a geometric perturbation on the inner cylinder.

A comprehensive literature survey of 3-D buoyancy-driven flow was presented by Vafai and Ettefagh [2]. Therefore, a brief overview of selected works concerned with different geometric modifications to the concentric cylindrical annulus having a finite axial length is presented here. Two-dimensional investigations were carried out by Kwon *et al.* [3], Zhang *et al.* [4] and Lai [5]. Kwon *et al.* [3] carried out a study of natural convection in the annulus between horizontal circular cylinders with three axial spacers which were equally spaced. The variation in flow pattern, temperature distribution and heat transfer were studied by varying the Rayleigh number, Prandtl number, diameter-ratio and the location and thermal conductivity of the axial spacers. The heat transfer across the annulus was found to be strongly affected by the conduction through the spacers. Zhang *et al.* [4] presented the results of an experimental study of laminar natural convection fluid flow and heat transfer in the horizontal annulus between a cylindrical envelope and its concentric octagonal heated inner cylinder. The octagonal cylinders investigated include one with a complete surface and the other with horizontal slots on the top and bottom surfaces. Smoke was used to visualize the flow and it revealed that while the flow pattern for the unslotted case was very similar to that in a concentric cylindrical annulus, it was quite different for the case of the slotted cylinder. They found that significant heat transfer enhancement was obtained for the slotted case. Lai [5] numerically investigated the feasibility of using radial baffles to improve the effectiveness of pipe insulation. The objective was to reduce heat transfer by natural convection in the horizontal annulus. Three baffle designs, namely full baffles, partial inner baffles, and partial outer baffles

† Author to whom correspondence should be addressed.

NOMENCLATURE

D_1	diameter of inner cylinder [m]
D_2	diameter of outer cylinder [m]
g	acceleration due to gravity [m s^{-2}]
k	thermal conductivity [W m^{-1} K^{-1}]
L	total length of the annulus [m]
L_1	length of the portion of the annulus without the perturbation [m]
L_p	length of the portion of the annulus with the perturbation [m]
Nu	Nusselt number
n	outward drawn normal
Pr	Prandtl number, ν/α
p	pressure [Pa]
R_1	radius of the inner cylinder [m]
R_2	radius of the outer cylinder [m]
R_p	radius of the perturbation [m]
Ra	Rayleigh number $g\beta(R_2-R_1)^3\Delta T/\nu\alpha$
T	temperature [K]
u_x	velocity in the x-direction [m s^{-1}]
u_y	velocity in the y-direction [m s^{-1}]
u_z	velocity in the z-direction [m s^{-1}]
r	radial coordinate [m]
x, y, z	Cartesian coordinates [m].

Greek symbols

α	thermal diffusivity [m^2 s^{-1}]
β	coefficient of volume expansion [K^{-1}]
ν	kinematic viscosity [kg m^{-1} s^{-1}]
μ	dynamic viscosity [m^2 s^{-1}]
ρ	density [kg m^{-3}].

Subscripts

1	inner cylinder
2	outer cylinder
p	perturbation
x	x-component
y	y-component
z	z-component
∞	condition at infinity
Φ	circumferential coordinate, degrees.

were considered. The study of the relation between the heat loss and the baffle orientation angle for each pipe–baffle configuration revealed that radial baffles were effective in reducing the heat loss and the effectiveness increased with increase in baffle number.

The main objective of this work is to provide a qualitative and a quantitative understanding of the flow field and the corresponding heat transfer process in a cylindrical annulus subject to a geometric perturbation. A thorough understanding of the buoyancy-induced flow-field and heat transfer in this geometry will provide a strong basis for identifying the local maxima and minima of convective energy transfer, and thereby, will be an important design tool. The heat transfer behavior is studied by looking at the variations in the average and the local Nusselt numbers on the inner and the outer cylinders. Another objective of the current study is to study the effect of variation of key geometric parameters of the perturbation, like the size and aspect-ratio. In order to quantify the effects of these parameters, correlations have been obtained for the average Nusselt number. The full 3-D Navier–Stokes equation is solved numerically using the Galerkin weighted residual method of the finite-element formulation.

In the next section, the selection of the basic geometry and the analysis used to understand the flow field are presented. The definitions of the local and the average Nusselt numbers are provided and the detailed explanations for their variations are given. The discussions are made with respect to the corresponding case for the annulus without the perturbation so that the distinct features and the effect of the inclusion of the perturbation are seen clearly. The effects of the variations in the geometric parameters and the development of the correlations for the average Nusselt number are discussed.

2. FORMULATION

2.1. *Physical model and assumptions*

The physical model and coordinate system used in the present study is shown in Fig. 1. Due to the symmetric nature of the flow field in the axial direction, only half the axial length of the annulus is considered in the analysis. In a given half of the annulus, the lengths of the portions with and without the perturbation are L_p and L_1 respectively. The radius of the inner cylinder in the $0 \leqslant x \leqslant L_1$ region of the annulus is R_1 while that of the perturbation in the $L_1 \leqslant x \leqslant L_p$ region is R_p. The outer radius of the annulus is R_2. The flow is going to be symmetric with respect to the vertical plane crossing the center of the cylinders and hence the region of interest is half the annulus.

The thermophysical properties of the walls and the fluid are assumed to be independent of temperature in the analysis, except for the density in the buoyancy term. The fluid is assumed to be Newtonian and incompressible. The Boussinesq approximation is invoked and the viscous heat dissipation in the fluid is neglected.

2.2. *Governing equations*

The problem is modeled as a 3-D, steady-state, natural convection in an incompressible fluid. The non-dimensional governing equations are:

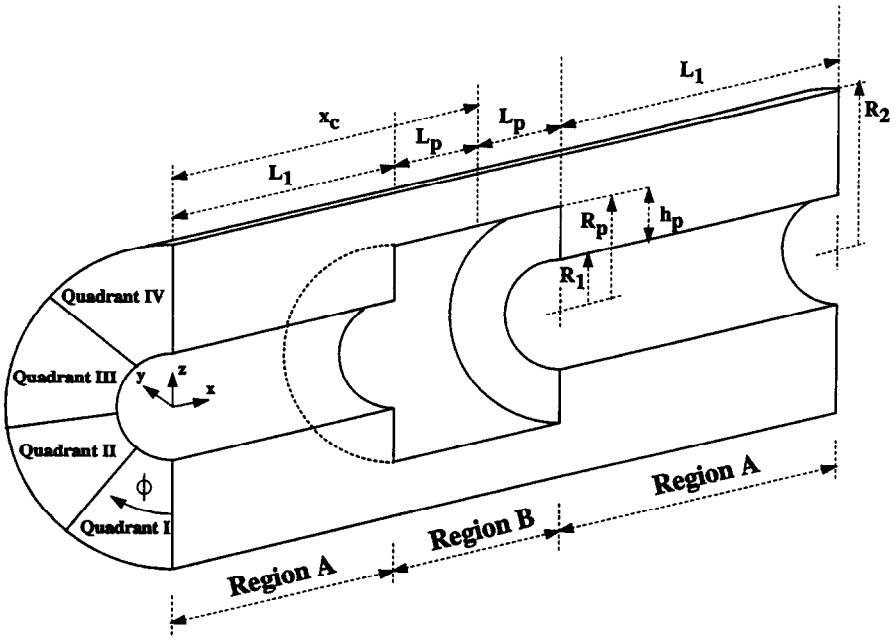

Fig. 1. Schematic of model used in analysis.

continuity

$$\frac{\partial u_x}{\partial x}+\frac{\partial u_y}{\partial y}+\frac{\partial u_z}{\partial z}=0; \tag{1}$$

x momentum

$$\left(\frac{Ra}{Pr}\right)^{1/2}\left\{u_x\frac{\partial u_x}{\partial x}+u_y\frac{\partial u_x}{\partial y}+u_z\frac{\partial u_x}{\partial z}\right\}=-\frac{\partial p}{\partial x}+\nabla^2 u_x; \tag{2}$$

y momentum

$$\left(\frac{Ra}{Pr}\right)^{1/2}\left\{u_x\frac{\partial u_y}{\partial x}+u_y\frac{\partial u_y}{\partial y}+u_z\frac{\partial u_y}{\partial z}\right\}=-\frac{\partial p}{\partial y}+\nabla^2 u_y; \tag{3}$$

z momentum

$$\left(\frac{Ra}{Pr}\right)^{1/2}\left\{u_x\frac{\partial u_z}{\partial x}+u_y\frac{\partial u_z}{\partial y}+u_z\frac{\partial u_z}{\partial z}\right\}=-\frac{\partial p}{\partial z}+\left(\frac{Ra}{Pr}\right)^{1/2}T+\nabla^2 u_z; \tag{4}$$

energy

$$\left(\frac{Ra}{Pr}\right)^{1/2}\left\{u_x\frac{\partial T}{\partial x}+u_y\frac{\partial T}{\partial y}+u_z\frac{\partial T}{\partial z}\right\}=\nabla^2 T. \tag{5}$$

The following dimensionless parameters have been used and the superscripts have been dropped for convenience.

$$x^*=\frac{x}{R_2}\quad y^*=\frac{y}{R_2}\quad z^*=\frac{z}{R_2} \tag{6}$$

$$u_x^*=\frac{u_xR_2}{\alpha(RaPr)^{1/2}}\quad u_y^*=\frac{u_yR_2}{\alpha(RaPr)^{1/2}}\quad u_z^*=\frac{u_zR_2}{\alpha(RaPr)^{1/2}} \tag{7}$$

$$T^*=\frac{T-T_\infty}{T_1-T_\infty}\quad p^*=\frac{pR_2^2}{\nu\alpha(RaPr)^{1/2}} \tag{8}$$

These five equations in terms of the five unknowns, namely u_x, u_y, u_z, p and T along with the appropriate boundary conditions fully describe the buoyancy-driven flow in the annulus.

2.3. *Boundary conditions*

Across the axial symmetry plane, there is no fluid flow and also no heat transfer. Similarly, there is no flow of fluid or heat across the vertical symmetry plane. The left end wall is assumed to be insulated. On all rigid and impermeable surfaces, the three components of velocity are zero. The boundary conditions are summarized below.

(1) For the left end wall:

$$\text{at } x=0 \quad \text{and} \quad \frac{R_1}{R_2}\leqslant r\leqslant 1$$

$$u_x=u_y=u_z=0,\quad \frac{\partial T}{\partial x}=0. \tag{9}$$

(2) For the axial symmetry plane:

$$\text{at } x = \frac{L_1 + L_p}{R_2} \quad \text{and} \quad \frac{R_p}{R_2} \leqslant r \leqslant 1,$$

$$u_x = 0, \quad \frac{\partial T}{\partial x} = 0. \tag{10}$$

(3) For the vertical symmetry plane:

$$\Phi = 0^\circ \quad \text{and} \quad \Phi = 180^\circ$$

$$0 \leqslant x \leqslant \frac{L_1}{R_2} \quad \text{and} \quad \frac{R_1}{R_2} \leqslant r \leqslant 1$$

$$\frac{L_1}{R_2} \leqslant x \leqslant \frac{(L_1 + L_p)}{R_2} \quad \text{and} \quad \frac{R_p}{R_2} \leqslant r \leqslant 1$$

$$u_y = 0, \quad \frac{\partial T}{\partial y} = 0. \tag{11}$$

(4) For the curved surface of the inner cylinder:

$$\text{at } r = \frac{R_1}{R_2} \quad \text{and} \quad 0 < x \leqslant \frac{L_1}{R_2},$$

$$u_x = u_y = u_z = 0, \quad T = \frac{T_1 - T_\infty}{T_1 - T_\infty} = 1. \tag{12}$$

(5) For the vertical surface of the perturbation:

$$\text{at } x = \frac{L_1}{R_2} \quad \text{and} \quad \frac{R_1}{R_2} < r < \frac{R_p}{R_2}$$

$$u_x = u_y = u_z = 0, \quad T = \frac{T_1 - T_\infty}{T_1 - T_\infty} = 1. \tag{13}$$

(6) For the curved surface of the perturbation:

$$\text{at } r = \frac{R_p}{R_2} \quad \text{and} \quad \frac{L_1}{R_2} \leqslant x < \frac{(L_1 + L_p)}{R_2}$$

$$u_x = u_y = u_z = 0, \quad \text{and} \quad T = \frac{T_1 - T_\infty}{T_1 - T_\infty} = 1. \tag{14}$$

(7) For the curved surface of the outer cylinder:

$$\text{at } r = 1 \quad \text{and} \quad 0 \leqslant x \leqslant \frac{(L_1 + L_p)}{R_2}$$

$$u_x = u_y = u_z = 0, \quad T = \frac{T_2 - T_\infty}{T_1 - T_\infty}. \tag{15}$$

2.4. *Numerical scheme*

The cited coupled nonlinear system of governing equations along with the described boundary conditions were discretized using the Galerkin method of weighted residuals as described in the FIDAP Theoretical Manual [6]. The important aspects of the numerical scheme are briefly outlined in this section. The continuum domain is first divided into elements within each of which, the unknown variables u, v, w, p and T are approximated using interpolation functions. Substitutions of these approximations into the governing equations and boundary conditions yields a residual in each of these equations and the Galerkin form of the method of weighted residuals seeks to reduce these errors to zero in a weighted sense. This results in a global system of algebraic equations over the entire domain. The segregated solution algorithm was selected to solve the system of equations. In a segregated formulation, the global discretized equation, which is in the form of a global system matrix, is decomposed into smaller submatrices and then solved in a sequential manner. This results in considerably lesser storage requirements as compared to that required for the storage of the global system matrix. Since the computation resource requirement for the direct solvers become prohibitively large for large-scale simulations, iterative solvers were used in the present study. The conjugate residual (CR) scheme was used to solve the symmetric pressure type equation systems, while the conjugate gradient squared (CGS) scheme was used for the nonsymmetric advection–diffusion type equations.

2.5. *Computational details*

A finer mesh was used in regions where steeper gradients were expected. This practice was adopted near the walls within the annulus. The mesh size was determined after considerable numerical experimentation. For the annulus with the perturbation located at the centre, a grid-structure consisting of about 20 000 elements was found to be sufficient to produce a grid-independent solution. With the perturbation at the centre, only half the annulus length was considered due to the axial symmetry. However, for some of the cases in the current study, in which the perturbation is not located at the centre of the annulus, the entire length of the annulus had to be considered in the analysis, and for these cases, grid-independent solutions were obtained with about 35 000 elements.

3. FLOW AND HEAT TRANSFER RESULTS

3.1. *Fluid flow*

3.1.1. *Background.* For the case of natural convection in the annulus between horizontal concentric cylinders of infinite axial length, Kuehn and Goldstein [1] obtained a two-dimensional crescent shaped vortex. However, for many practical applications, the annulus has a finite axial length. This necessitates a three-dimensional analysis to take care of the viscous-shearing effects at the end-walls. The effect of the shear force at the walls is also felt in the middle portion of the annulus. Takata *et al.* [7] studied the natural convection in an inclined cylindrical annulus for very high Prandtl number fluids. Their study revealed that a fluid particle which is introduced at the left end of the annulus moves in the axial-direction from the starting point, drawing a small crescent-shaped vortex in the r-Φ plane. As the particle approaches the central region of the annulus, its velocity in the axial direction was found to decrease gradually with an increase in

the size of the crescent shape. The particle was then found to turn in the opposite direction and move towards the starting point by drawing a larger crescent-shaped vortex outside the smaller one. Such a trace of fluid particle was called a co-axial helix, which was essentially the same structure obtained by Vafai and Ettefagh [2]. It should be noted that for an inclined cylindrical annulus with heating and cooling at the end plates, Ozoe *et al.* [8] also obtained a similar structure. The main objective of the current study is to obtain a thorough understanding of the effects of the inclusion of a geometric perturbation on the flow field within an annulus.

Since one of the objectives of this investigation was to compare the numerical solution with previous works [1, 2], the outer cylinder to inner cylinder ratio was taken as 2.6 and the ratio of the axial length to outer radius was considered to be 4.0. The outer radius of the annulus was taken as 1.0, and the length of the perturbation in the axial direction was considered to be 0.8 (thereby making $L_1 = 1.6$ and $L_p = 0.4$ in a half-length of the annulus).

3.1.2. *Representation of the flow-field.* From an initial survey of the velocity vector field, the highly three-dimensional nature of the flow-field was revealed. In order to understand the flow-field, a systematic approach was adopted which is briefly outlined below.

A comprehensive probe into the flow-behavior within the annulus is done. For the description of the flow-field and the heat transfer behavior, the cylindrical coordinate system (r, Φ, x) has been adopted for the sake of convenience. A comprehensive study of numerical results revealed that over the domain of the annulus, the flow-field could be broadly disintegrated into two clear regions: a region over the relatively narrow portion of the annulus formed between the perturbation and the outer cylinder (region B) and that over the remaining portion of the annulus (region A). For convenience, the two regions identified above will henceforth be referred to as region A and region B (Fig. 1).

At a given axial plane, the crescent-shaped flow pattern is observed but it varies considerably in the axial direction. Within the regions A and B, the axial component of the velocity could be subdivided into distinct circumferential pockets. This behavior lead to the utilization of averaging of the axial component over the circumferential direction. For clarity in presenting the flow-field results, the circumferential averaging was done over four quadrants.

3.1.3. *Essential features of the flow.* The essential features of the flow-field are presented in Fig. 2 for the region A and Fig. 3 for region B. The four figures for each region represent the variation in the axial component of the velocity averaged over each of the four quadrants, respectively. The discussion is presented for a Rayleigh number of 10 000, but all the main characteristics discussed here do apply for a wide range of Rayleigh numbers.

Concentrating on the first quadrant of the annulus, very little activity is observed at the left end of the annulus. However, a steady increase in the strength of the axial flow is observed towards the perturbation (Fig. 4). This can be attributed to the presence of the heated vertical portion of the perturbation. This heated vertical section causes the fluid in its vicinity to rise rapidly, thereby entraining fluid from the lower left end of the region A. As seen in Fig. 2(a), in the region closer to the inner cylinder, the axial-velocity has a negative component, which is due to the impingement of the flow in the vertical walls of the perturbation. Another aspect to be noted in Fig. 2(a) is that the flow has a strong axial component as it leaves region A and enters region B.

The flow which leaves region A along the bottom portion of the annulus finds its way into region B as can be seen in Fig. 3(a). As expected, the flow weakens as it approaches the axial symmetry plane. The fluid which was entrained by the heated vertical portion of the perturbation enters region B through the fourth quadrant from region A. This can be clearly seen in Figs. 4 and 3(d). Again, the flow weakens as it approaches the axial-symmetry plane.

As expected, the magnitude of the axial component of the velocity vanishes for the flow which enters region B from region A through the bottom and top portions of the annulus. As can be seen in Fig. 3(b,c), the fluid returns towards region A though the second and third quadrants. These figures show that as the returning fluid moves out towards region A from the axial-symmetry plane, the magnitude of the axial component of the velocity increases. A closer look at Fig. 3(b,c) will show that the speed of the returning flow is higher in the upper half of the annulus and it gradually diminishes as it moves towards the left end wall.

Another distinct feature of the flow-field is the counterclockwise rotating cell which is formed near the top left end of the annulus (Fig. 4). The flow-field for the regular annulus without a perturbation displays a similar behavior. The cause of this cell can be attributed to the viscous end-effects. The leftward moving flow along the outer cylinder eventually impinges the left end wall, thereby triggering-off the formation of the cell. It should be noted that at the mid-axial location, there is a confluence of three strong flow-pockets as seen in Fig. 4. One is the counter-clockwise cell which was just discussed. Another pocket is related to the flow from region B through the upper half of the annulus. The third flow pocket is the rising portion of the crescent in the r–Φ plane at that axial location. As a result of these interactions, a clockwise rotating cell is generated. There also exists a counter-clockwise rotating cell near the circumferential symmetry plane (Fig. 4) which is formed by that part of the flow entrained from the lower half of the annulus in region A which did not enter region B from region A. These clockwise and counter-clockwise rotating cells impinge in the region near the top of the

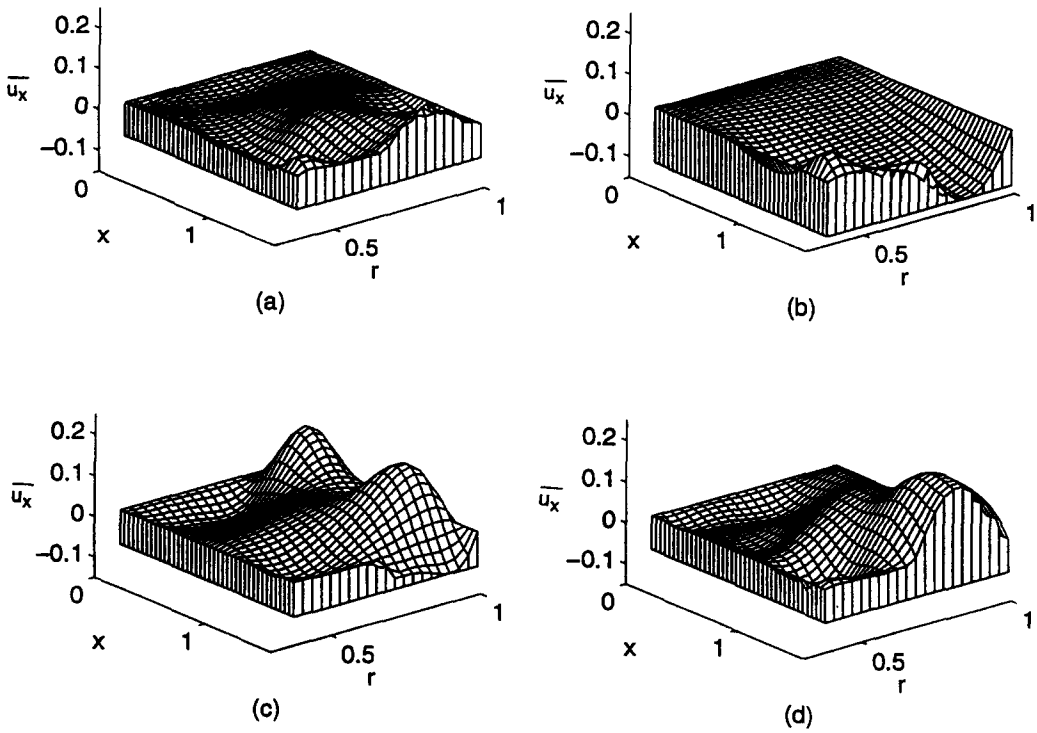

Fig. 2. Circumferentially-averaged axial velocities over the four quadrants: (a) quadrant I; (b) quadrant II; (c) quadrant III; and (d) quadrant IV in region A.

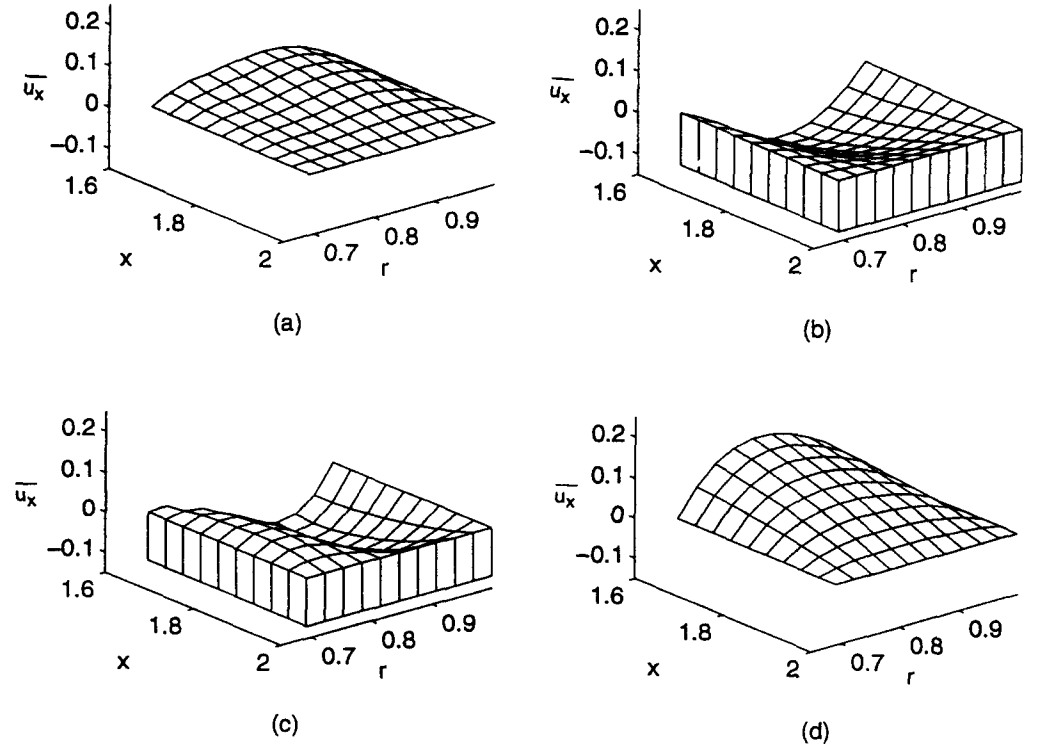

Fig. 3. Circumferentially-averaged axial velocities over the four quadrants: (a) quadrant I; (b) quadrant II; (c) quadrant III; and (d) quadrant IV in region B.

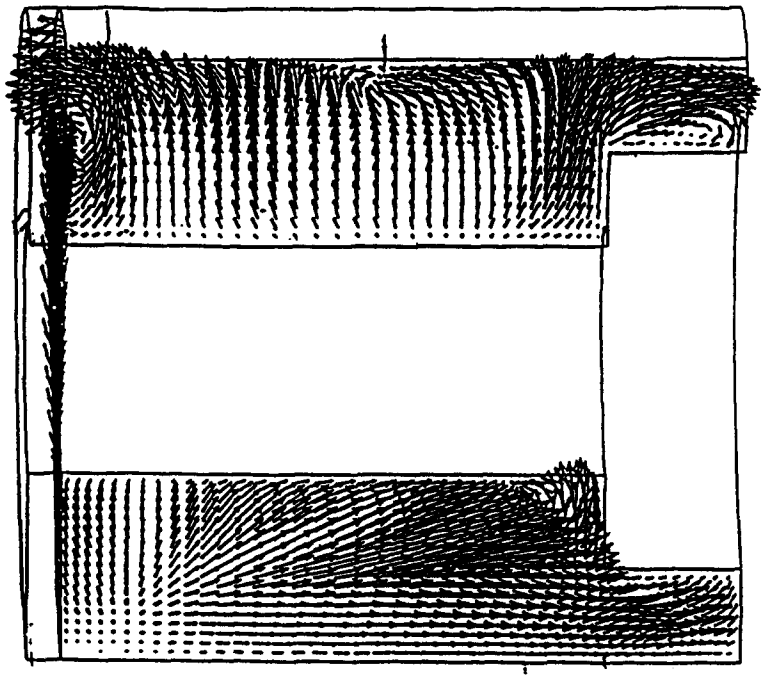

Fig. 4. Velocity vectors at circumferential symmetry plane.

circumferential symmetry plane to form a stagnation zone.

Thus it is seen that the nature of the flow field for the present study is considerably different from the coaxial double helix flow pattern of the regular annulus without a perturbation [2].

3.2. *Heat transfer*

The local Nusselt numbers for the inner and the outer cylinders are given by

$$Nu_{\text{inner}} = \frac{h_1 D_1}{2k} \ln\left(\frac{D_2}{D_1}\right)$$

$$\text{and} \quad Nu_{\text{outer}} = \frac{h_2 D_2}{2k} \ln\left(\frac{D_2}{D_1}\right) \tag{16}$$

where h_1 and h_2 are the local heat transfer coefficients on the inner and the outer cylinders and are, respectively, given by

$$h_1 = \frac{q_{w1}}{(T_1 - T_2)} \quad \text{and} \quad h_2 = \frac{q_{w2}}{(T_1 - T_2)} \tag{17}$$

where q_{w1} and q_{w2} are the heat fluxes per unit area form the inner and the outer cylinder surfaces, respectively.

These nondimensional heat fluxes are given by

$$q_w = \frac{\partial T}{\partial n} \tag{18}$$

when n denotes the normal pointing outwards from the surface over which the Nusselt number is to be calculated.

On the curved surface of the perturbation, the Nusselt number is given by

$$Nu_{\text{pert}} = \frac{1}{(T_1 - T_2)} \left(\frac{D_p}{2k}\right) \frac{\partial T}{\partial n} \ln\left(\frac{D_2}{D_{\text{pert}}}\right) \tag{19}$$

and the average Nusselt number over a surface area is given by

$$\overline{Nu} = \frac{1}{A} \int \frac{\partial T}{\partial n} \mathrm{d}A. \tag{20}$$

3.2.2. *Local Nusselt number distribution.* The distribution of the local Nusselt number for the inner and the outer cylinder as a function of the circumferential and the axial coordinates at a Rayleigh number of 10^4 is shown in Fig. 5. The local Nusselt number variations for the regular annulus without the perturbation are shown in Fig. 5(a,b), while Fig. 5(c,d) represents the local Nusselt number variations for the annulus with a perturbation. In Fig. 5(c), the local Nusselt number on the vertical face of the perturbation has not been shown. Only the variations on the curved surface of the inner cylinder and the perturbation have been shown since the objective of this illustration is to highlight the differences in important trends as compared to the case of the regular annulus without the perturbation. A first glance at the results show the same general trend for both the cases, i.e. the annulus with and without the perturbation. However, there are some regions of the annulus where the Nusselt number varies considerably between the two cases, thereby necessitating a more detailed discussion. This discussion has been subdivided into separate sections for the inner and the outer cylinder.

Inner cylinder

By comparing the local Nusselt number plots for the inner cylinder, the first notable difference is seen

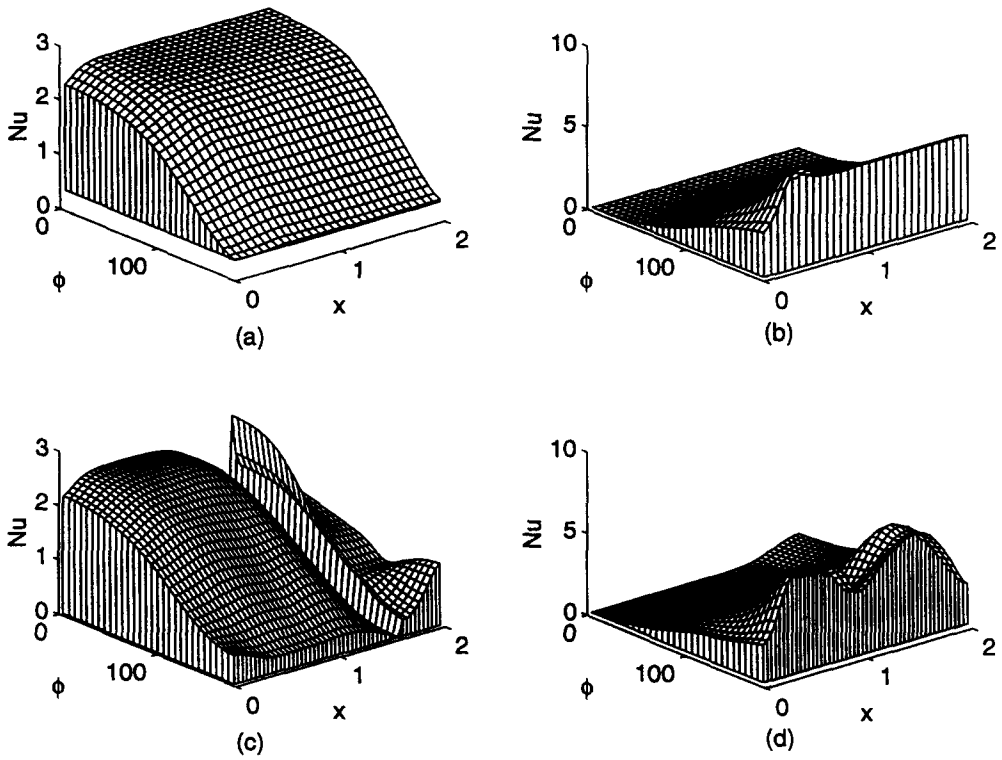

Fig. 5. Local Nusselt number distribution at $Ra = 10^4$: regular annulus—(a) inner cylinder; (b) outer cylinder annulus with perturbation—(c) inner cylinder; (d) outer cylinder.

at the axial location where the perturbation begins. From Fig. 2(a–d), it can be clearly seen that the flow undergoes a reversal after it strikes the vertical portion of the perturbation resulting in a significant reduction in the overall flow speed and hence a reduction in the local Nusselt number.

Inclusion of the perturbation introduces a number of effects as seen in region B of the annulus. The Nusselt number is found to increase from the plane where the perturbation begins to the axial symmetry plane. A careful study of the flow-field in this region reveals that as the entrained fluid from the lower half of region A enters region B through the upper half of the annulus, separation occurs along the horizontal surface of the perturbation. As the flow moves into region B, the separation near the horizontal surface of the perturbation decreases, accounting for the local Nusselt number increase in that region.

At the axial symmetry plane, the Nusselt number decreases near a circumferential location of $\Phi = 135°$ and then increases along the top of the annulus. This behavior can be attributed to the formation of a stagnant zone in that portion of the axial symmetry plane. The stagnation zone is formed by the impingement of opposing flows entering this pane from the top and bottom portions of the annulus, see Fig. 6.

Outer cylinder

A comparison of the local Nusselt number plots at the outer cylinder for the two cases shows some similar trends. The Nusselt number increases from the bottom to the top of the annulus. However, some notable differences in the local Nusselt number were seen near the top of the annulus. For the regular annulus, the viscous effects near the end-wall were seen at the top of

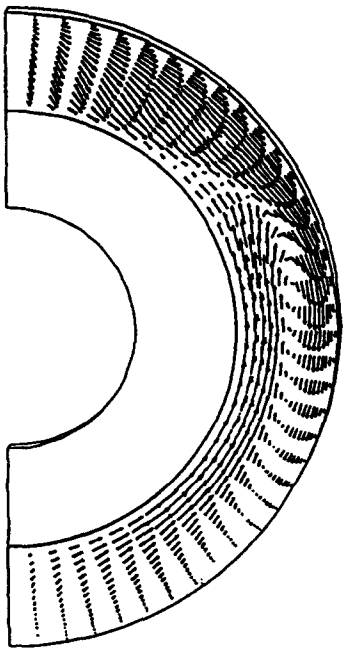

Fig. 6. Velocity vectors at axial symmetry plane.

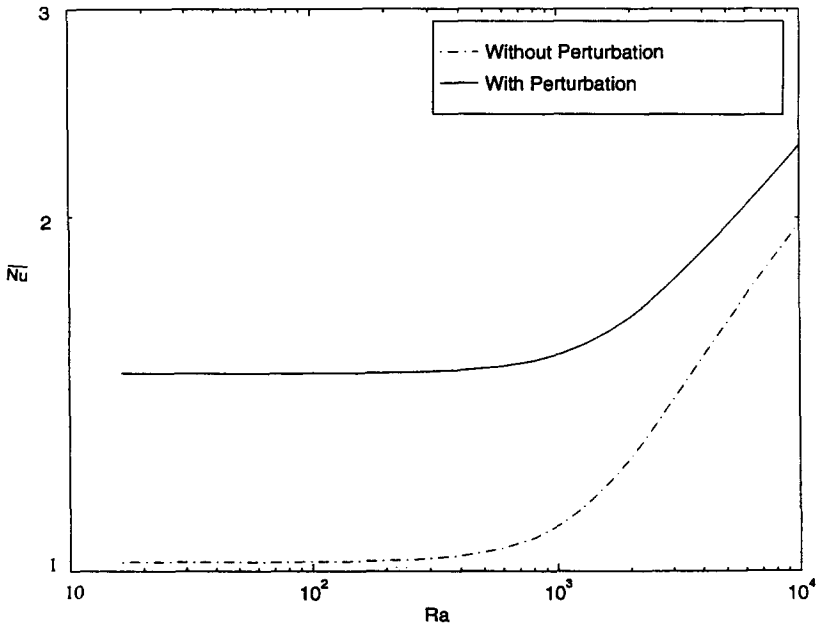

Fig. 7. Comparison of average Nusselt numbers for an annulus with and without a geometric perturbation.

the annulus whereas for the perturbation case, several maxima were seen. This behavior near the top region of the annulus is due to the different convection cells and flow patterns in this region. As for the regular annulus without a perturbation, the local Nusselt number increases from the left end wall.

The decrease in the local Nusselt number at the mid-axial location can be attributed to the presence of the stagnation zone formed in this region. Further, the impingement of the flow entrained from the lower portion of region A on the outer cylinder causes an increase in the Nusselt number. As the axial symmetry plane is approached, the Nusselt number is again seen to decrease.

3.3. *Overall heat transfer behavior*

To assess the overall effect of the perturbation on the heat transfer process, the average Nusselt number characteristics are analyzed. Figure 7 shows the average Nusselt number as a function of the Rayleigh number for the two cases. It is important to note that heat transfer enhancements of about 50% are obtained with the introduction of the perturbation within the annulus. The average Nusselt number variations as a function of the Rayleigh number can be correlated by the following equations.

For the regular annulus:

$$\overline{Nu} = 0.16Ra^{0.27} \text{ for } 10^3 \leqslant Ra \leqslant 10^4. \quad (21)$$

For the annulus with a perturbation at the centre:

$$\overline{Nu} = 0.39Ra^{0.19} \text{ for } 10^3 \leqslant Ra \leqslant 10^4. \quad (22)$$

It may be observed that the first correlation is identical to that obtained by Kuehn and Goldstein [1]. The numerical technique employed in the current study was validated by comparing the solutions of the limiting case without perturbations and comparing them with previous works [1, 2]. Excellent qualitative and quantitative agreement were observed.

4. EFFECTS OF VARIATIONS OF PERTINENT GEOMETRIC PARAMETERS

In this section, the influence of some key geometric parameters on the heat transfer performance will be studied. The geometric parameters which will be considered are the lengths of the geometric perturbation in the axial and the radial directions, the axial position of the perturbation in the annulus, and the gap-width between the inner and the outer cylinders. Dimensionless parameters used in characterizing the effects of the geometric parameters identified above are now given (Fig. 1).

(1) Dimensionless length of the perturbation in the axial direction is given by

$$x^* = \frac{2L_p}{L} \quad (23)$$

(2) Dimensionless length in the radial direction is given by

$$r^* = \frac{h_p}{G} \quad (24)$$

where $h_p = R_p - R_i$ and $G = R_2 - R_1$. In the above equation, R_1 and R_2 are the radii of the inner and the outer cylinder of the annulus, respectively, and R_p is the radius of the perturbation.

(3) The position of the perturbation in the annulus

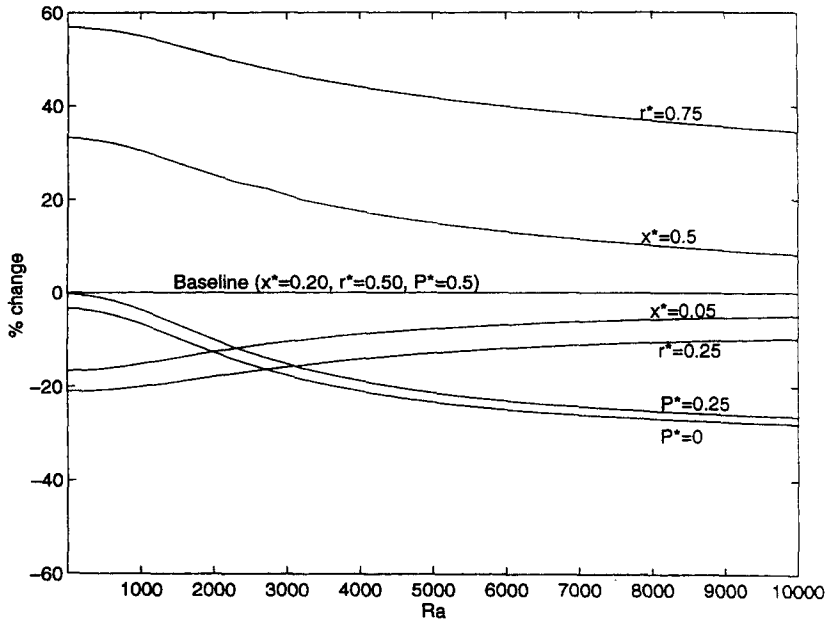

Fig. 8. Effect of variation in pertinent geometric parameters: % change in mean Nusselt compared to that for the baseline case.

is characterized by considering the axial distance between the left end wall of the annulus and the centre of the perturbation. Dimensionless axial position of the perturbation is given by

$$P^* = \frac{x_c - L_p}{L - 2L_p} \tag{25}$$

where x_c is the axial distance of the centre of the perturbation from the left end-wall. As the perturbation is moved from the left to the right end-wall, the value of P^* will change from 0 to 1.

(4) Dimensionless gap-width between the inner and the outer cylinder is given by

$$G^* = \frac{(R_2 - R_1)}{R_1}. \tag{26}$$

In order to study the effects of these geometric parameters, several cases were investigated. For each case, the average Nusselt number was compared with that for a baseline configuration. The geometric parameter for the baseline configuration and those for the different cases which were studied are summarized in the following table.

	x^*	r^*	P^*	G^*
Baseline	0.20	0.50	0.50	0.80
Case 1	0.05	0.50	0.50	0.80
Case 2	0.50	0.25	0.50	0.80
Case 3	0.20	0.75	0.50	0.80
Case 4	0.20	0.50	0.00	0.80
Case 5	0.20	0.50	0.25	0.80
Case 6	0.20	0.50	0.50	0.50
Case 7	0.20	0.50	0.50	0.10

The results obtained are shown in Fig. 8 in terms of the percentage change in average Nusselt number between each of the cases identified above and the baseline case. At any given Rayleigh number, the average Nusselt number was found to increase with an increase in the axial and the radial lengths of the perturbation. As seen in the figure, the effect of the axial and the radial dimensions of the perturbation decrease with an increase in Rayleigh number i.e. at a lower Rayleigh number, the effects of change in perturbation-dimensions are more prominent than those at higher Rayleigh numbers. As the axial length of the perturbation was reduced to 0.05 from the baseline dimension of 0.2, the average Nusselt number decreased by about 10–15% while it increased by about 10–30% when the axial dimension increased to 0.5. On the other hand, as the radial dimension was decreased from the baseline value of 0.5 to 0.25, the average Nusselt number decreased by about 15–20% while it increased by about 40–55% as the radial dimension was increased to 0.75 from the baseline value of 0.5. As the position of the perturbation in the annulus is moved progressively towards the left end-wall from the central location, the average Nusselt number was found to decrease. For example, when the perturbation is at the extreme left end-location, the average Nusselt number was found to decrease only marginally at Rayleigh numbers up to about 10^3, while it decreased by as much as 25% as the Rayleigh number approached 10^4. For the perturbation located at a quarter-annulus length from the left end, the heat transfer behavior was quite similar to the case where the perturbation was at the left end wall. While studying the effect of the gap-width, it has to be noted that

the gap-width appears in the definition of the Rayleigh number and so its effect on the heat transfer performance was considered separately. As the gap-width is changed from a baseline value of 0.80 to 0.5, the average Nusselt number deceases by about 5% while it decreases by about 15% for a gap width of 0.1.

The results can be well coordinated by the following equation:

$$\overline{Nu} = 0.30Ra^{0.08}(1+0.62x^*)(1+2.67r^*) \times (1+0.69P^*)Pr^{-0.01} \quad (27)$$

which is valid for $10^3 \leqslant Ra \leqslant 10^4$ and $0.7 \leqslant Pr \leqslant 100$. Equation (27) captures the effects of all the pertinent geometric parameters as well as the Rayleigh number and Prandtl number variations.

5. CONCLUSION

Buoyancy-induced flow and heat transfer in a cylindrical annulus in the presence of a geometrical perturbation is investigated in this work. The general patterns and the detailed features of the flow and heat transfer in the annulus due to the perturbation are presented. The detailed 3-D structure of the flow field and heat transfer characteristics within this type of geometry has been analyzed and compared with that of the regular cylindrical annulus without any perturbation. With the introduction of the perturbation in the annulus, the flow field differed considerably from the coaxial double helix flow pattern of the regular annulus. It was found that the introduction of a geometric perturbation can result in considerable increase in the overall heat transfer.

The effects of some key geometric parameters of the perturbation on the heat transfer characteristics were studied. The influence of the length of the perturbation in the axial and radial directions, the axial position of the perturbation in the annulus and that of the gap-width between the inner and the outer cylinders have been studied. The average Nusselt number was found to increase with an increase in the axial and radial lengths of the perturbation. As the perturbation is moved from the central axial location to either end, the rate of increase in the average Nusselt number due to the perturbation was found to decrease. However, the presence of the perturbation regardless of the location induced a significant increase in the overall heat transfer within the annulus. As the gap width between the inner and the outer cylinders decreased, the average Nusselt number was found to decrease. Considering the effect of the perturbation on the flow and heat transfer within the annulus, this work could serve as an initial design tool for a number of practical applications which were mentioned earlier.

REFERENCES

1. Kuehn, T. H. and Goldstein, R. J., An experimental and theoretical study of natural convection in the annulus between horizontal concentric cylinders. *Journal of Fluid Mechanics*, 1976, **74,** 695–719.
2. Vafai, K. and Ettefagh, J., An investigation of transient three-dimensional buoyancy-driven flow and heat transfer in a closed horizontal annulus. *International Journal of Heat and Mass Transfer*, 1991, **34,** 2555–2570.
3. Kwon, S. S., Kuehn, T. H. and Lee, T. S., Natural convection in the annulus between horizontal circular cylinders with three axial spacers. *Journal of Heat Transfer*, 1982, **104,** 118–124.
4. Zhang, H. L., Wu, Q. J. and Tao, W. Q., Experimental study of natural convection heat transfer between a cylindrical envelope and an internal concentric heated octagonal cylinder with or without slots. *Journal of Heat Transfer*, 1991, **113,** 116–121.
5. Lai, F. C., Improving effectiveness of pipe insulation by using radial baffles to suppress natural convection. *International Journal of Heat and Mass Transfer*, 1993, **36,** 899–906.
6. *FIDAP Theoretical Manual.* Fluid Dynamics International, Evanston, IL, 1993.
7. Takata, Y., Iwashige, K., Fukuda, K. and Hasegawa, H., Three dimensional natural convection in an inclined cylindrical annulus. *International Journal of Heat and Mass Transfer*, 1984, **27,** 745–754.
8. Ozoe, H., Shibata, T. and Churchill, S. W., Natural convection in an inclined circular cylindrical annulus heated and cooled on its end plates. *International Journal of Heat and Mass Transfer*, 1981, **24,** 727–737.